BILINGUAL PUBLISHING CO.
Pioneer of Global Academics Since 1984

Journal of Environmental & Earth Sciences
https://ojs.bilpublishing.com/index.php/jees

ARTICLE

Metamorphic Evolution of the Amphibolites from Bundelkhand Craton, Central India: *P-T* Constraints and Phase Equilibrium Modelling

Pratigya Pathak* **Shyam Bihari Dwivedi** **Ravi Ranjan Kumar**

Department of Civil Engineering, Indian Institute of Technology (BHU), Varanasi, India

ARTICLE INFO

Article history
Received: 24 January 2022
Accepted: 17 March 2022
Published Online: 6 April 2022

Keywords:
Bundelkhand craton
Amphibolite
P-T pseudosection
Subduction setting

ABSTRACT

The amphibolites from the Mauranipur and Babina regions are located in the central part of the Bundelkhand Craton (BuC), northern India. During the geodynamic evolution of the BuC, these amphibolites underwent medium-grade metamorphism. This study combines textural observations of amphibolites from two distinct regions (Mauranipur and Babina) with mineral chemistry and phase equilibrium modelling. Observations suggest that the amphibolites of both areas have gone through three stages of metamorphism. The pre-peak stage in the amphibolites from the Mauranipur and Babina regions is marked by the assemblages Ep-Amp-Cpx-Pl-Ilm-Ru-Qz and Ep-Amp-Cpx-Pl-Ab-Ilm-Qz respectively; the peak metamorphic stage is characterized by the mineral assemblages Amp-Cpx-Pl-Ilm-Ru-Qz and Amp-Cpx-Pl-Ilm-Qz-H_2O, which is formed during the burial process, and the post-peak stage is represented by the assemblages Amp-Pl-Ilm-Ru-Qz and Amp-Pl-Ilm-Qz-H_2O respectively, which is formed by exhumation event. By applying the phase equilibria modelling in the NCFMASHTO system, the *P-T* conditions estimated from pre-peak, peak to post-peak stages are characterized as 6.7 kbar/510 °C, 7.3 kbar/578 ºC and > 3.0 kbar/> 585 ºC, respectively, for the Mauranipur amphibolites; and 6.27 kbar/520 ºC, 5.2 kbar/805 ºC and > 3.0 kbar/> 640 ºC respectively for Babina amphibolites. The textural association and *P-T* conditions of both amphibolites suggest that these rocks were affected by burial metamorphism followed by an exhumation process during subduction tectonism in the BuC.

1. Introduction

Continental crust formation began in the Hadean ages (4.4 Ga-4.0 Ga), as reported by the Acasta gneisses of northwestern Canada [1-3]. However, the current continental crust was developed through multiple mechanisms and stages before 2.5 Ga [4-6]. The Archean cratons have been well-known for their ability to provide insight into Earth's earlier crustal history. These Archean cratons contain a

*Corresponding Author:
Pratigya Pathak,
Department of Civil Engineering, Indian Institute of Technology (BHU), Varanasi, India;
Email: pratigyapathak.rs.civ17@itbhu.ac.in

DOI: https://doi.org/10.30564/jees.v4i1.4397

variety of igneous rocks that exhibit structural indicators, as well as supracrustal rocks such as amphibolites, tonalite-trondhjemite-granodiorite gneisses (TTGs), and banded iron formations (BIFs) displaying various metamorphic stages [7]. Supracrustal rocks contributed significantly to the formation of microcontinents, supercontinents, continental evolution, and the stabilization of continents [8-10]. As a result, the metamorphic study of supracrustal rocks is tremendously beneficial and required for a better understanding of geodynamic evolution and stabilization of cratons and continental crust.

The Bundelkhand Craton (BuC) is located in the northern Indian Shield and is also the best example of an Archean craton for studying supracrustal rocks because it contains a record of geological events from the Archean (3.5 Ga-2.7 Ga; TTGs and gneisses) to the Paleoproterozoic (2.5 Ga-2.4 Ga; granitoid pulses) periods [11-13]. Despite that, the BuC experienced various metamorphic events, and it preserves medium to high-grade metamorphism in multiple rock types. *P-T* conditions of 5.4 kbar/730 °C and 6.2 kbar/720 °C have been reported from the Mauranipur metapelites [14,15]. Similarly, high-grade hornblende-biotite-plagioclase bearing gneisses of *P-T* = 6.5-8.5 kbar/630-720 °C has been reported in the Sukwan (Babina) area [16]. High to ultrahigh-pressure metamorphism is reported in chlorite-phlogopite-corundum schists with *P-T* condition as 11 kbar/630 °C and 18 kbar/630 °C respectively, from the Babina region [11]. The garnet-bearing BIF from the Mauranipur region reveals a peak temperature of ~500 °C at 0.1 GPa-0.2 GPa, suggesting lower amphibolite facies [17]. The peak metamorphic condition of garnet-biotite gneiss has been revealed as 6.35-6.75 kbar/755-780 ºC [18]. Several authors concluded that the mafic and ultramafic rocks of the BuC underwent greenschist to amphibolite facies metamorphism based on textural and mineralogical observations [19,20]. Field investigations imply that amphibolites are connected with multiple metamorphic Archean terrains, and hence, understanding the geological history of that terrain requires a complete understanding of amphibolites. Amphibolites have been reported from various cratons in the Indian shield. Amphibolites (hornblende-garnet-epidote-glaucophane-augite-chlorite) have been reported from the Nagaland Ophiolite Complex, with *P-T* conditions of 13.8 kbar-12.6 kbar and 625 °C-645 °C [21]. However, low-pressure amphibolites (amphibole-plagioclase-biotite-quartz-garnet-chlorite-epidote-magnetite) have also been delineated from the Western Dharwar Craton with *P-T* conditions of 5 kbar/600 °C [22].

One of the most contentious and exciting issues in metamorphic petrology has always been the origin of amphibolites. These rocks have a variety of origins and have been determined to be the most difficult in nature, as well as playing a significant role in revealing the history of Archean terrain crustal evolution [23]. Amphibolites are thought to be formed from igneous rocks of basic and tholeiitic magma that represent pieces of earlier oceanic crust. Amphibolites can also be produced by metasomatism of calcareous sediments [24]; some amphibolites can be formed from pre-existing rocks that have undergone a succession of mineral and chemical transformations as a result of metamorphism [21]. Most researchers believe that three processes, namely meta-igneous, meta-sedimentary, and metasomatism, are the most valid mechanisms for the production of amphibolites [25]. However, multiple mechanisms have been reported to give rise to amphibolites hence predicting the origin of different amphibolites is the most debated and intriguing subject in metamorphic petrology.

To better understand the metamorphic development of amphibolites from the BuC, we used petrographical study, mineral chemistry of numerous minerals, and phase equilibria modelling of amphibolites from the Mauranipur and Babina regions. The field evidence of amphibolites and textural relationship of existing minerals are explained in this study, as well as pseudosection modelling is used to create the *P-T* trajectory paths.

2. Geological Backgrounds

The Indian shield comprises two cratonic blocks, namely the northern cratonic block consisting of Aravalli and Bundelkhand cratons, and the southern cratonic block, which includes Dharwar, Bastar, and Singhbhum cratons [26] (Figure 1a). The BuC has a semi-circular shape and is located in the north-central section of the Indian subcontinent covering a 30,000 km^2 area [27]. It is separated from the southern cratonic block by the Central Indian Tectonic Zone (CITZ) [9]. The BuC is separated from the Aravalli Craton by the NE-SW trending Great Boundary Fault (GBF) and from the Himalaya by the Yamuna Fault. The BuC is covered by Indo-Gangetic alluvium in the north, by Vindhyan rocks in the east as well as south, and by Deccan basalts in the southwest [28] (Figure 1b). The Paleoproterozoic (2.0 Ga-1.8 Ga) peripheral sedimentary basins of Gwalior, Sonrai, and Bijawar border the BuC from the northwest, south, and southeast, respectively [29]. These basins are homotaxial, with clastic sedimentary rocks at the bottom and carbonate with banded iron formations (BIFs) at the top [30].

The BuC was primarily created throughout the Paleoarchean to Neoarchean periods, with the multistage crustal formation. The BuC is divided into two crustal segments

by an E-W trending Bundelkhand Tectonic Zone (BTZ) that runs roughly 200 kilometres from Mahoba to Babina (Figure 1b). The first segment is the central domain, known as the central Bundelkhand greenstone terrane (CBGT), and the second is the southern domain, known as the southern Bundelkhand greenstone terrane (SBGT) [30]. NW-SE trending mafic dykes of Proterozoic age (~1.98 Ga, 1.8 Ga, and 1.0 Ga) and NE-SW trending quartz veins of Palaeoproterozoic age (1.9 Ga-1.8 Ga) dissect the whole BuC.

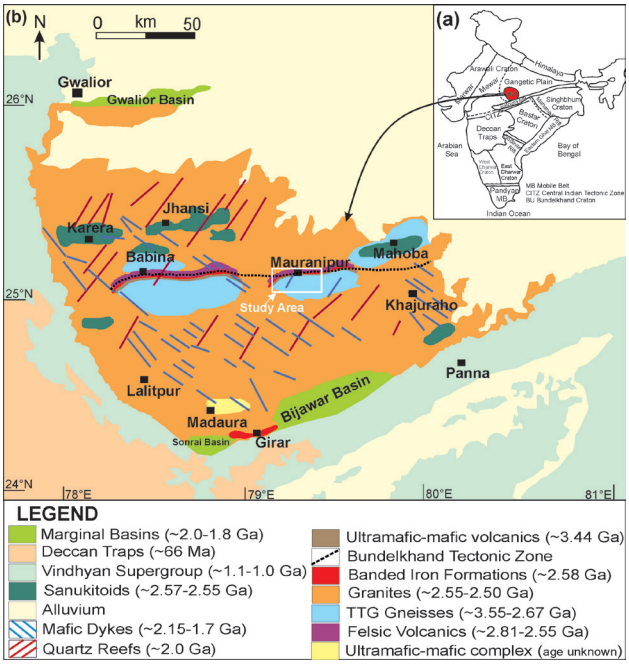

Figure 1. (a) Inset map showing the location of the Bundelkhand Craton in India. (b) The geological map shows different lithological units and tectonic elements of the Bundelkhand Craton [30].

The CBGT is mainly dominated by Tonalite-Trondhjemite-Granodiorite (TTG) gneisses of Mesoarchean age, greenstones of Neoarchean age, intrusive granites, quartz reefs, mafic dykes, BIFs, and metabasites [16,31]. The CBGT, mostly exposed in the Babina and Mauranipur regions, contains metamorphosed mafic rocks of the Paleo-Mesoarchean period [28], felsic volcanic rocks of the Mesoarchean period [32] and metasedimentary rocks (BIFs). Ultramafic-mafic volcanic rocks from the Babina and Mauranipur regions have been emplaced during the Paleoarchean age (3.44 Ga) [31]. This volcanism is likely to have occurred after the emplacement of TTGs (3.55 Ga-3.20 Ga) in a subduction scenario from a depleted mantle source. Pink granites and granodiorites (2.58 Ga-2.52 Ga) cross this belt in various directions, indicating an intrusive link with CBGT rocks [33]. According to available geochronological data [34], the CBGT has been formed during three stages of volcanic activity. Early felsic volcanic activity occurred in the Mauranipur region around 2.82 Ga, implying Mesoarchean subduction tectonics [34]. At 2.54 Ga, a new period of volcanic activity was identified in the Babina region [34], whereas the third stage has culminated during ~2.5 Ga by the accretion of massive continental chunks [31].

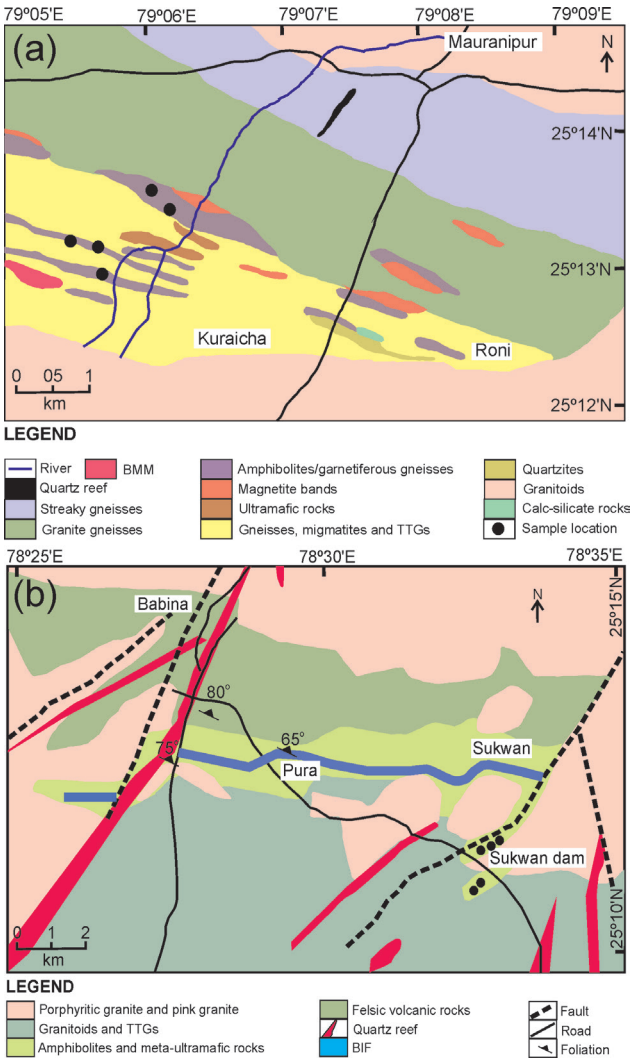

Figure 2. (a) Local geological map of the study area around Mauranipur region [19]. (b) Local geological map around the Babina region, elucidating various geological occurrences [47].

3. Field and Megascopic Description

The amphibolite samples were collected from a variety of locations in the Babina and Mauranipur regions. Amphibolites were exposed in the Mauranipur (Lattitude 25º11'54" N to 25º14'48" N, Longitude 79º05' S to 79º09'35" S; Figure 2a) as well as in the Babina region (Lattitude 25º09'45" N to 25º15' N, Longitude 78º25' S to 78º35'S; Figure 2b). Amphibolites are found as enclaves

within TTG gneisses and felsic granitoid (Figure 3a), but they have also been seen as intrusive dykes in TTG gneisses in the Mauranipur and Babina regions (Figure 3b). Amphibolites have been found associated with a variety of rock types, including BIF, calc-silicate rocks, white schists, quartzites, and metapelites. Mauranipur amphibolites are found with garnetiferrous gneisses, whereas Babina amphibolites are associated with meta-ultramafic rocks. Amphibolites from both sites have a nematogranoblastic texture that overwrites all previous textures and structures [32]. The amphibolites are primarily dark in colour and reveal a fractured nature in several areas of the research field (Figure 3b). Amphibolites from the Mauranipur region show a massive emplacement of felsic magmatism (Figure 3c) with folded and distorted structures (Figure 3d). Babina amphibolites (near the Sukwa-Dukwa dam) resemble Mauranipur amphibolites in appearance and are likewise intruded by felsic magma (Figure 3e,f).

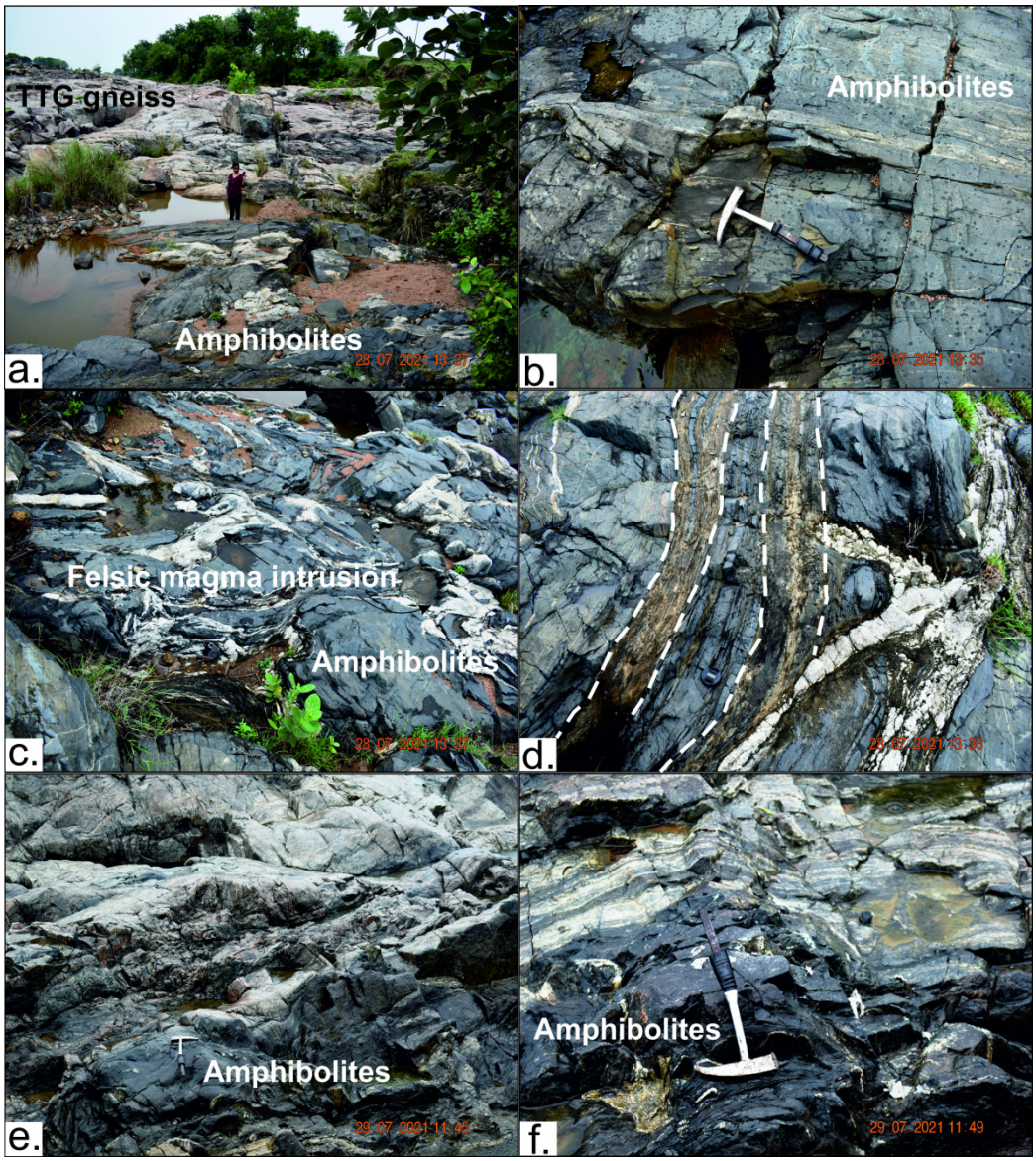

Figure 3. Field photographs of the amphibolites from the study area (a) Amphibolites exposed along with TTG gneisses in Mauranipur, (b) Small scale field photograph of amphibolites along with deformational features in Mauranipur, (c) Felsic magma intrusion in amphibolites of Mauranipur (d) Folding in the layers of amphibolites of Mauranipur (e,f) Amphibolites of Babina (near Sukwa-dukwa dam) intruded by felsic magma.

4. Petrography

The principal minerals in amphibolites from both regions are amphibole, clinopyroxene, and plagioclase, with K-feldspar, epidote, quartz, and opaque minerals (rutile, ilmenite, and magnetite) occurring as accessory phases. Table 1 shows the mineral assemblages and modal abundances of various amphibolite samples from the Mauranipur and Babina regions. The mineral assemblages' paragenesis is as follows:

a. Amphibole-clinopyroxene-plagioclase-rutile-epidote-ilmenite-quartz

b. Amphibole-clinopyroxene-plagioclase-albite-epidote-ilmenite-quartz

c. Amphibole-clinopyroxene-plagioclase-rutile-ilmenite-quartz

d. Amphibole-clinopyroxene-plagioclase-ilmenite-quartz

e. Amphibole-plagioclase-rutile-ilmenite-quartz

f. Amphibole-plagioclase-ilmenite-quartz

The petrographical investigation of amphibolites from both samples MM-1 and BB-1 has revealed three different modes of occurrence of amphiboles. These all three amphiboles have characteristics features and textural association, which are depicted in the following way; the inclusion-type amphibole (Amp1) enclosed in clinopyroxene, the porphyroblastic amphibole (Amp2) associated with clinopyroxene crystals, and the retrograde amphibole (Amp3) replacing clinopyroxene crystal. The first-generation amphibole (Amp1) is light brown to green color and occurs as inclusions within porphyroblast clinopyroxene, intergrown with plagioclase, a textural feature indicating that Amp1 is a result of the prograde metamorphism (Figure 4a,b). Porphyroblastic and subhedral grains of amphiboles are considered as the second generation of amphiboles (Amp2), closely associated with clinopyroxene porphyroblast; and textural features suggest that it would be a product of peak metamorphism (Figure 4c,d). The Amp2 has a green color and contains inclusions of discrete plagioclase, quartz, and ilmenite, representing sieve texture. Amphibole crystals are mainly medium to coarse-grained in nature as well as subhedral to anhedral in shape depicting two sets of cleavage, present with porphyroblasts of clinopyroxene (Figure 4c). Green to grey clinopyroxene up to 1 cm in length, intergrown with plagioclase, displays an ophitic texture (Figure 4d). The textural relationship of amphibole replacing clinopyroxene suggests retrograde metamorphism (Figure 4e,f). This petrographical evidence indicates that the third generation of amphibole (Amp3) is preserved in the studied amphibolites. Plagioclase is an essential mineral in amphibolites, and it records essential metamorphic information. The plagioclase is fine to medium-grained 0.1 mm-0.2 mm in size and anhedral shape and is characterized by colorless prismatic crystals and first-order grey color. In spite of the presence of the plagioclase as inclusion within clinopyroxene and amphibole, it also occurs as the dominant phase of the matrix (Figure 4g). Epidotes occur as < 50 µm rounded subhedral crystals associated with amphibole and plagioclase but mostly appeared as inclusion within amphibole and clinopyroxene crystals (Figure 4a,b). Plagioclase can also be found as an inclusion inside the amphibole and clinopyroxene matrix (Figure 4h). At the confluence of amphibole and plagioclase, Figure 4i displays a lengthy lath of ilmenite.

Table 1. Summary of approximate modal composition (in percentage) of the Amphibolites of Mauranipur (MM-1, MM-2, MM-3, MM-4, MM-5) and Babina (BB-1, BB-2, BB-3, BB-4, BB-5) samples observed under a petrological microscope through Lieca Qwin software.

Sample	Model %						
	Amp	Cpx	Pl	Kfs	Ep	Qz	Opq
MM-1	52	30	6	1	4	1	6
MM-2	49	32	8	-	3	2	6
MM-3	53	27	5	2	4	1	8
MM-4	50	33	7	1	4	1	4
MM-5	55	21	10	1	5	1	7
BB-1	48	33	8	2	3	1	5
BB-2	52	24	11	-	3	2	8
BB-3	51	29	9	1	5	1	4
BB-4	53	35	5	1	2	1	3
BB-5	54	31	9	1	2	1	2

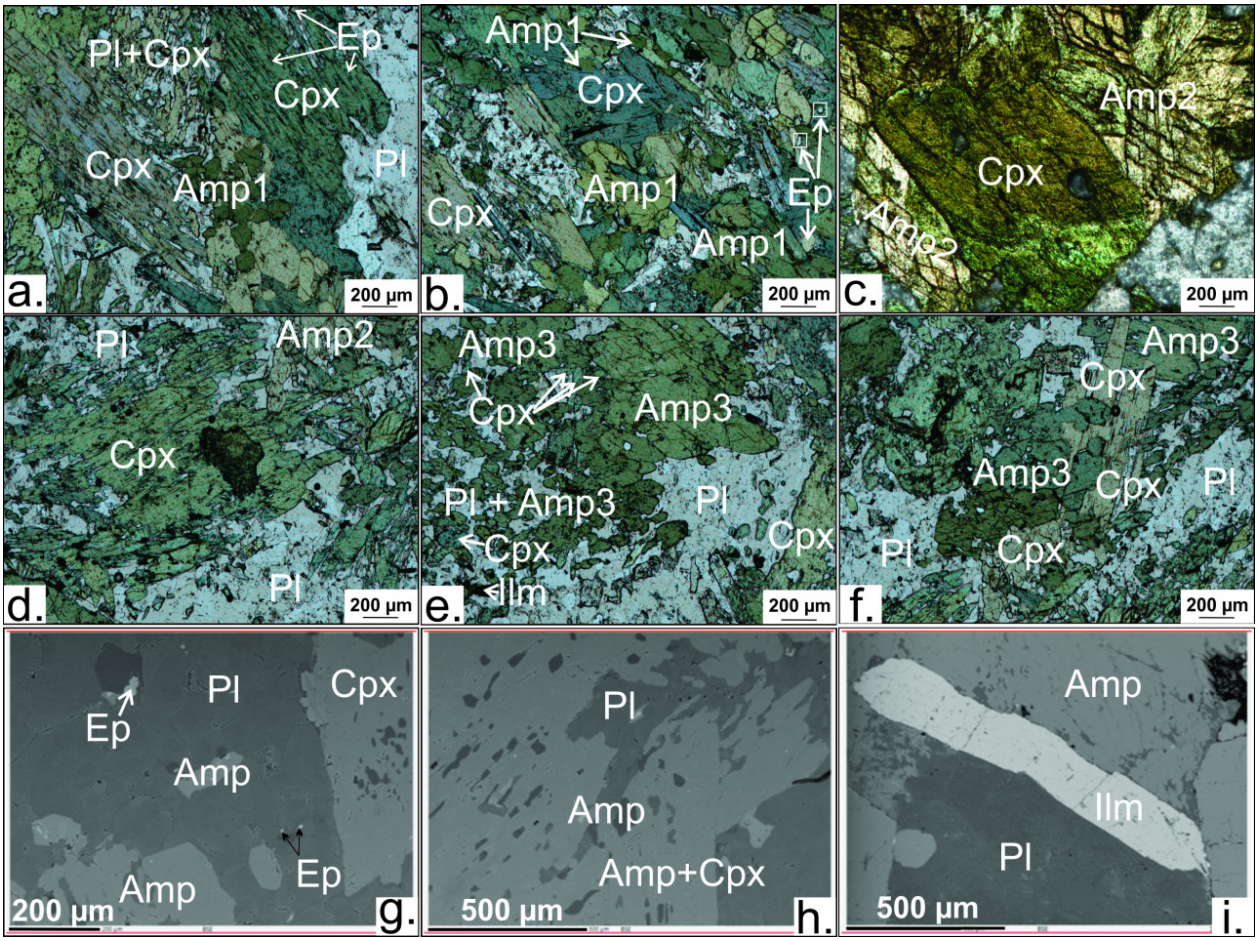

Figure 4. Photomicrographs (plane-polarized light, PPL) and back-scattered electron (BSE) images of the amphibolites (MM-1 and BB-1): (a & b) First generation Amp1 and Ep present as inclusions in Cpx with Pl, (c) Prismatic crystals Amp2 depicting two sets of cleavage with porphyroblastic Cpx, (d) Laths of Pl embedded within Cpx crystals depicting ophitic texture, (e) Third generation Amp3 contains inclusions of Cpx, (f) Cpx crystals partially replaced by third-generation Amp3, (g) Ep crystals occurring as inclusions within Amp and Pl, (h) Pl present as inclusion within the matrix of Amp and Cpx, (i) Long lath shaped grain of Ilm at a junction of Amp and Pl. Mineral abbreviations are taken from Whitney and Evans [49].

5. Mineral Chemistry

5.1 Analytical Method

Based on petrological interpretations, two amphibolite samples, namely MM-1 (from Mauranipur) and BB-1 (from Babina), were selected for the electron microprobe analysis (EPMA). The mineral chemical analysis was carried out using the EPMA (CAMECA SX five EPMA) at the Department of Geology, Banaras Hindu University, Varanasi, India, under operating conditions of 15 kV and the current 10 nA.

5.2 Amphibole

All the analysed amphiboles (sample MM-1 and BB-1) have (Na + K) < 0.50, Ti < 0.5, CaB > 1.5 pfu. Furthermore, according to Leak's, classification [35], these are Ca-amphibole groups in composition. When the analyzed amphiboles are plotted on the leaks classification diagram, they all occupy the tschermakite and Mgnesio-hornblende domains (Figure 5a). All the analyzed amphiboles (sample MM-1 and BB-1) based on 23 oxygens are presented in Table 2. Amp1 has a value of 0.75 for X_{Mg} [Mg/(Fe^{2+}+Mg)], Amp2 has a value of 0.78-0.79, and Amp3 has a value of 0.71-0.72 for the sample MM-1. The X_{Ca} values range from 0.31-0.33 for the amphiboles of MM-1. The sample BB-1 also includes three types of amphibole, compositionally distinct, and their X_{Mg} values are 0.71-0.74 for Amp1, 0.79-0.82 for Amp2 and 0.68-0.69 for Amp3.

Table 2. EPMA (wt%) and structural formula of amphibole, from the Amphibolites of Mauranipur and Babina (Sample MM-1 and BB-1).

Sample	**MM-1**						**BB-1**					
Domain	5/1	6/1	7/1	8/1	22/1	25/1	43/1	45/1	46/1	47/1	50/1	52/1
Position	Amp1		Amp2		Amp3		Amp1		Amp2		Amp3	
SiO_2	43.40	43.56	43.62	43.66	44.68	44.27	43.96	43.72	44.81	43.66	44.32	45.30
TiO_2	0.41	0.39	0.42	0.50	0.43	0.42	0.48	0.35	0.40	0.43	0.44	0.41
Al_2O_3	14.22	14.32	14.87	13.41	12.94	13.61	13.10	14.83	12.20	16.08	14.62	13.50
FeO	12.11	12.14	11.95	14.21	12.41	13.03	13.77	12.13	13.50	11.58	13.65	13.28
MnO	0.26	0.10	0.06	0.18	0.23	0.33	0.16	0.18	0.10	0.11	0.16	0.24
MgO	11.89	12.13	12.57	12.30	11.99	11.55	11.81	11.83	12.93	12.33	11.12	11.41
CaO	11.65	11.68	11.92	11.64	11.69	11.26	11.98	11.84	11.74	11.44	11.80	11.34
Na_2O	1.38	1.59	1.33	1.62	1.49	1.69	1.35	1.29	1.39	1.50	1.37	1.66
K_2O	0.18	0.17	0.20	0.18	0.21	0.18	0.25	0.21	0.17	0.19	0.23	0.20
Total	95.49	96.07	96.93	97.69	96.06	96.34	97.56	97.12	97.24	97.32	97.70	97.35
23 oxygens												
Si	6.37	6.36	6.28	6.29	6.55	6.46	6.42	6.36	6.46	6.23	6.40	6.56
Al^{IV}	1.63	1.64	1.72	1.71	1.45	1.54	1.58	1.64	1.54	1.77	1.60	1.44
Al^{VI}	0.83	0.82	0.81	0.57	0.78	0.81	0.67	0.90	0.54	0.94	0.89	0.86
Ti	0.05	0.04	0.05	0.05	0.05	0.05	0.05	0.04	0.04	0.05	0.05	0.05
Fe^{3+}	0.61	0.59	0.73	0.95	0.44	0.60	0.62	0.58	0.87	0.79	0.53	0.48
Fe^{2+}	0.87	0.89	0.71	0.76	1.08	0.99	1.06	0.90	0.76	0.59	1.11	1.13
Mn	0.03	0.01	0.01	0.02	0.03	0.04	0.02	0.02	0.01	0.01	0.02	0.03
Mg	2.60	2.64	2.70	2.64	2.62	2.52	2.57	2.57	2.78	2.62	2.39	2.46
Ca	1.83	1.83	1.84	1.80	1.84	1.76	1.88	1.84	1.81	1.75	1.83	1.76
Na	0.39	0.45	0.37	0.45	0.42	0.48	0.38	0.36	0.39	0.41	0.38	0.47
K	0.03	0.03	0.04	0.03	0.04	0.03	0.05	0.04	0.03	0.03	0.04	0.04
X_{Mg}	0.75	0.75	0.79	0.78	0.71	0.72	0.71	0.74	0.79	0.82	0.68	0.69

$X_{Mg} = Mg/(Fe^{2+} + Mg)$

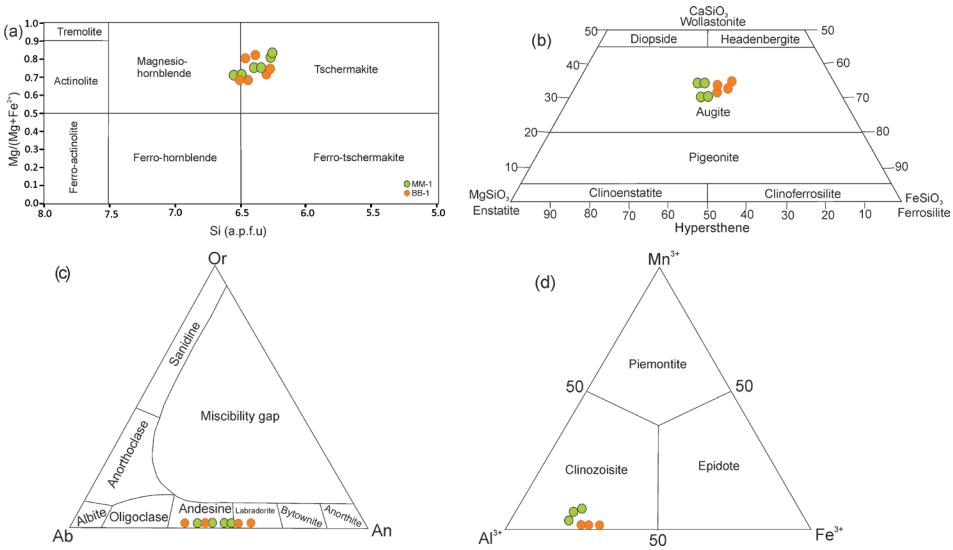

Figure 5. (a) Plots of the analyzed amphiboles obtained from the amphibolites of Mauranipur and Babina on classification diagram [35], (b) Pyroxene classification diagram showing the augite nature of the clinopyroxenes, from both amphibolites [36], (c) Plots of the orthoclase-albite-anorthite ternary diagram, showing andesine and labradoritic nature, (d) Plots of the ternary epidote diagram [37].

Table 3. EPMA (wt%) and structural formula of clinopyroxenes, from the Amphibolites of Mauranipur and Babina (Sample MM-1 and BB-1).

Sample	**MM-1**				**BB-1**			
Domain	11/1	12/1	13/1	14/1	23/1	44/1	45/1	88/1
SiO_2	49.22	49.55	48.89	47.45	48.25	48.74	47.24	48.56
TiO_2	0.14	0.12	0.16	0.1	0.10	0.15	0.18	0.16
Al_2O_3	0.49	0.55	0.77	0.5	0.60	0.99	0.55	0.47
Cr_2O_3	0.09	0.08	0.08	0.1	0.10	0.07	0.02	0.01
FeO	23.79	21.2	23.26	21.34	22.30	23.15	24.16	22.78
MnO	0.22	0.33	0.23	0.24	0.30	0.23	0.45	0.34
MgO	8.12	10.11	8.29	11.43	9.92	8.45	8.79	9.22
CaO	17.22	17.65	17.66	18.52	17.56	17.56	18.22	18.05
Na_2O	0.12	0.13	0.11	0.02	0.10	0.1	0.01	0.12
K_2O	0	0.02	0.01	0	0.00	0.01	0.02	0.01
Total	99.41	99.74	99.46	99.7	99.23	99.45	99.64	99.72
6 oxygens								
Si	1.96	1.95	1.95	1.89	1.92	1.94	1.90	1.93
Al	0.02	0.03	0.04	0.02	0.03	0.05	0.03	0.02
Cr	0.00	0.00	0.00	0.00	0.00	0.00	0.00	0.00
Ti	0.00	0.00	0.00	0.00	0.00	0.00	0.01	0.00
Fe^{3+}	0.07	0.11	0.09	0.29	0.18	0.10	0.23	0.17
Fe^{2+}	0.72	0.58	0.68	0.40	0.55	0.67	0.56	0.58
Mn	0.01	0.01	0.01	0.01	0.01	0.01	0.02	0.01
Mg	0.48	0.59	0.49	0.68	0.59	0.50	0.53	0.55
Ca	0.74	0.74	0.75	0.79	0.75	0.75	0.79	0.77
Na	0.01	0.01	0.01	0.00	0.01	0.01	0.00	0.01
K	0.00	0.00	0.00	0.00	0.00	0.00	0.00	0.00
X_{Mg}	0.40	0.51	0.42	0.63	0.52	0.43	0.48	0.48

$X_{Mg} = Mg/(Fe^{2+}+ Mg)$

5.3 Clinopyroxene

All the analyzed clinopyroxenes (sample MM-1 and BB-1) based on 6 oxygens are presented in Table 3. The calculated X_{Mg} value of clinopyroxene from amphibolites of the study area ranges from 0.40-0.63 (samples MM-1) and 0.43-0.52 (sample BB-1). The triangular plot [36] for the pyroxene end member shows clinopyroxenes from both sample plots in the augite composition field (Figure 5b). The Ca content of clinopyroxene ranged from 0.74 pfu to 0.79 pfu for sample MM-1 and from 0.75-0.77 pfu for sample BB-1, providing evidence of the high Ca content of clinopyroxene.

5.4 Plagioclase

Plagioclase in samples MM-1 and BB-1 has a wide range in anorthite content (Table 4). Plagioclases from both samples are dominated by anorthite and albite, with minor orthoclase. However, the plagioclase of sample MM-1 (An = 42.92 mol%-44.49 mol%, Ab = 55.06 mol%-56.67 mol%) has less content in anorthite and higher content in albite in comparison to sample BB-1, which has (An = 41.50 mol%-56.09 mol%, Ab = 43.55 mol%-58.32 mol%). Feldspar in both samples contains a small amount of total iron in the form of FeO (up to 0.47 in sample MM-1 and 0.16 in sample BB-1). The triangular plot for plagioclase end-members show that plagioclase is plotted in the andesine and labradorite composition fields from both samples (Figure 5c).

5.5 Other Minerals

Representative chemical compositions of the analyzed epidotes based on 25 oxygens for both the samples (MM-1 and BB-1) are listed in Table 5. As an inclusion within amphibole and clinopyroxene, epidote is present in both amphibolites (MM-1 and BB-1). Subtle variations are observed in the chemical composition of epidotes from both samples. The values of X_{Al} [X_{Al}= $Al/(Al+Fe^{3+})$] for

both representatives range from 0.84 to 0.85. All epidotes belong to the clinozoisite-epidote-piemontite series, and the triangular plot [37] (Figure 5d) shows that epidotes from both samples are dominated by clinozoisite composition (83.53 mol%-84.59 mol%) for sample MM-1, whereas it is 83.39 mol%-84.97 mol% for sample BB-1. Ilmenite reveals that TiO_2 content ranges between 49.87 wt%-50.15 wt% in sample MM-1 and 45.00 wt%-45.46 wt% in sample BB-1 (Table 6). Ilmenite minerals did not show zoning as analyses on different points on the same grain showed almost identical values supported by BSE images (Figure 4i).

Table 4. EPMA (wt%) and structural formula of plagioclase from Amphibolites (MM-1 and BB-1).

Sample	**MM-1**				**BB-1**			
Domain	37/1	38/1	39/1	40/1	144/1	142/1	149/1	150/1
SiO_2	56.53	56.13	56.24	55.38	55.08	54.38	55.39	56.82
Al_2O_3	25.17	27.24	27.31	27.38	27.58	27.78	26.70	25.69
FeO	0.47	0.00	0.00	0.00	0.00	0.00	0.13	0.16
CaO	9.92	9.58	9.24	9.87	11.41	12.10	9.44	9.82
Na_2O	6.92	6.65	6.74	6.75	5.53	5.19	7.33	6.47
K_2O	0.06	0.04	0.07	0.08	0.02	0.06	0.03	0.02
Total	99.07	99.63	99.60	99.47	99.61	99.52	99.03	98.98
8 Oxygens								
Si	2.58	2.53	2.54	2.51	2.50	2.47	2.53	2.58
Al	1.35	1.45	1.45	1.46	1.47	1.49	1.44	1.38
Fe^{2+}	0.02	0.00	0.00	0.00	0.00	0.00	0.00	0.01
Ca	0.48	0.46	0.45	0.48	0.55	0.59	0.46	0.48
Na	0.61	0.58	0.59	0.59	0.49	0.46	0.65	0.57
K	0.00	0.00	0.00	0.00	0.00	0.00	0.00	0.00
Total	5.05	5.03	5.03	5.05	5.01	5.01	5.08	5.01
An	44.06	44.24	42.92	44.49	53.21	56.09	41.50	45.54
Ab	55.63	55.56	56.67	55.06	46.67	43.55	58.32	54.36
Or	0.32	0.20	0.41	0.45	0.12	0.35	0.18	0.09

Table 5. EPMA (wt%) and structural formula of epidote, from the Amphibolites of Mauranipur and Babina (Sample MM-1 and BB-1).

Sample no.	**MM-1**			**BB-1**		
Domain	45/1	46/1	47/1	48/1	49/1	54/1
SiO_2	35.04	36.44	35.37	36.30	36.54	36.52
TiO_2	0.09	0.10	0.11	0.12	0.10	0.03
Al_2O_3	23.52	23.73	24.47	23.69	23.36	24.13
Fe_2O_3	13.89	13.90	13.74	12.85	14.11	13.20
MnO	0.28	0.15	0.10	0.12	0.21	0.11
CaO	23.31	22.47	22.55	23.05	22.77	23.11
Total	96.42	96.80	96.35	96.13	97.10	97.12
25 oxygens						
Si	6.14	6.31	6.16	6.29	6.33	6.27
Al	4.86	4.84	5.021	4.84	4.77	4.88
Ti	0.01	0.01	0.01	0.02	0.01	0.00
Fe^{3+}	0.92	0.91	0.90	0.84	0.92	0.85
Mn	0.04	0.02	0.01	0.02	0.03	0.02
Ca	4.38	4.17	4.21	4.28	4.22	4.25
Total	16.42	16.26	16.32	16.28	16.28	16.28
Cz	83.53	83.93	84.59	84.97	83.39	84.89
Ep	15.75	15.69	15.17	14.71	16.08	14.83
Pie	0.72	0.37	0.24	0.31	0.53	0.28
X_{Al}	0.84	0.84	0.85	0.85	0.84	0.85

$X_{Al} = Al/(Fe^{3+} + Al)$

Table 6. EPMA (wt%) and structural formula of rutile and ilmenite, from the Amphibolites of Mauranipur and Babina (Sample MM-1 and BB-1).

Sample no.	**MM-1**			**BB-1**		
Position	Rt	Ilm		Rt	Ilm	
Domain	51/1	14/1	20/1	56/1	21/1	27/1
SiO_2	0.09	0.23	0.01	0.09	0.03	0.00
TiO_2	99.46	49.87	50.15	99.46	51.15	51.10
FeO	0.49	45.31	44.82	0.49	45.46	45.00
MnO	0.05	0.89	1.08	0.05	1.20	0.50
CaO	0.44	0.05	0.09	0.44	0.09	0.15
V_2O_3	0.00	2.31	2.32	0.00	2.33	2.53
Total	100.54	98.87	98.55	100.54	100.38	100.04
3 oxygens						
Si	0.00	0.01	0.00	0.00	0.00	0.00
Ti	0.99	0.96	0.97	0.99	0.97	0.97
Fe^{3+}	0.00	0.03	0.02	0.00	0.02	0.00
Fe^{2+}	0.01	0.94	0.94	0.01	0.94	0.95
Mn	0.00	0.02	0.02	0.00	0.03	0.01
Ca	0.01	0.00	0.00	0.01	0.00	0.00
V	0.00	0.05	0.05	0.00	0.05	0.05
Total	1.01	2.00	2.00	1.01	2.00	2.01

6. Phase Equilibria Modelling

6.1 Analytical Method

The bulk rock chemical compositional analysis for the major oxides of the representative amphibolite samples of Mauranipur (MM-1) and Babina (BB-1) was performed at the Birbal Sahni Institute of Palaeosciences (BSIP), Lucknow, India. Major oxides were analyzed by X-ray fluorescence (XRF) using a wavelength dispersive (WD-XRF AXIOS MAX) machine with a power of 4 KW, 60 kV-160 mA analytical, on a pressed powder pellet machine using 'kameyo' at a pressure of 15-20 tones with a 4 mm pallet thickness.

6.2 *P-T* Pseudosection

Phase equilibria modelling was done by constructing *P-T* pseudosections for the representative amphibolites from the Mauranipur and Babina of the specific mineral assemblages. For this purpose, Perple_X ver.6.9.0 software [38,39] was used with an end-member thermodynamic dataset [40,41]. Various solution models were used for the pseudosection construction, such as clinopyroxene [42], amphibole [43], plagioclase [44], epidote [41] and ilmenite [45].

Pseudosections are generally constructed to decipher the equilibrium relationship among the various mineral phases in rocks at different metamorphic *P-T* conditions. Here, the *P-T* pseudosections for both amphibolites (MM-1 and BB-1) were calculated in the NCFMASHTO (Na_2O-CaO-FeO-MgO-Al_2O_3-SiO_2-H_2O-TiO_2-O_2) system, where P_2O_5 and MnO were removed due to their negligible amounts, and quartz was taken as a ubiquitous phase (Figures 6 and 7). Furthermore, because the sample contains no biotite, muscovite, or K-feldspar, the influence of K_2O on the T-X(H_2O) and *P-T* pseudosection diagrams was ignored. The measured whole-rock composition of MM-1 and BB-1 was normalized in mol%, represented in Tables 7 and 8, respectively. The H_2O content for both samples was derived with the help of T-X(H_2O) pseudosection; however, the O_2 was evaluated by the composition of mineral phases and their modal abundance present in the rock.

6.3 Sample MM-1

T-X(H_2O) diagram of sample MM-1 was built in order to specify the probable water content in stable constraints to distinct metamorphic stages and associated *P-T* requirements at 7.5 and 4.0 kbar, respectively. The H_2O content is determined by the variation of H_2O from 0.0 mol% to 6.0 mol% in the bulk rock composition (Figure 6a,b). In the NCFMASHTO system, the appropriate mole ratios of oxides are normalized to 100%, as shown in Table 7. As illustrated in Figures 6a and 6b, the epidote is unstable at lower H_2O values before breaching the Ep entry line

Table 7. Major element concentration (wt%) and calculated effective composition (mol%) of Amphibolites of Mauranipur (Sample MM-1).

Composition	(wt%)		$X(H_2O)=C_0$	$X(H_2O)=C_1$	(mol%)
SiO_2	50.27	SiO_2	52.52	49.83	50.42
Al_2O_3	15.50	Al_2O_3	9.54	8.98	9.16
CaO	8.36	CaO	9.35	8.80	8.98
MgO	7.90	MgO	12.30	11.81	11.81
FeO	11.27	FeO	9.84	9.26	9.45
Na_2O	3.78	Na_2O	3.83	3.61	3.68
TiO_2	1.33	TiO_2	1.04	0.98	1.0
LOI	1.60	H_2O	0	6	4.0
		O_2	1.56	1.47	1.50
Total	100.00	Total	100	100.0	100
Data used for figure			Figure 6a,b		Figure 6c,d

Table 8. Major element concentration (wt%) and calculated effective composition (mol%) of Amphibolites of Babina (Sample BB-1).

Composition	(wt%)		$X(H_2O)=C_0$	$X(H_2O)=C_1$	(mol%)
SiO_2	50.40	SiO_2	52.90	49.78	50.78
Al_2O_3	16.14	Al_2O_3	9.98	9.39	9.58
CaO	8.86	CaO	9.96	9.37	9.56
MgO	7.17	MgO	11.22	10.56	10.77
FeO	11.26	FeO	9.89	9.30	9.49
Na_2O	3.86	Na_2O	3.93	3.70	3.77
TiO_2	0.73	TiO_2	0.57	0.54	0.55
LOI	1.59	H_2O	0.00	6.00	4.00
		O_2	1.56	1.47	1.50
Total	100.00	Total	100	100.0	100
Data used for figure			Figure 7a,b		Figure 7c,d

(yellow line). The solid red line indicates the appearance of H_2O as the temperature increases. The pre-peak stage mineral assemblage Ep-Amp-Cpx-Pl-Ilm-Ru-Qz is stable in $X(H_2O)$ values of 0.72-0.85 (long dashed black line). The observed mineral assemblage of the peak stage, Amp-Cpx-Pl-Ilm-Ru-Qz, is stable for $X(H_2O)$ values 0.61-0.65, while the mineral assemblage of the post-peak stage Amp-Pl-Ilm-Ru-Qz does not appear at a higher pressure of 7.5 kbar, this is most likely due to the pressure value chosen being too high (Figure 6a). When the T-$X(H_2O)$ diagram is calculated at lower pressure values of 4.0 kbar, the post-peak stage mineral assemblage appears (Figure 6b). Hence, we chose an $X(H_2O)$ value of 4.00, which was calculated on the basis of effective composition (Table 7) and then normalized to 100% by considering stable fields of mineral assemblages for pre- peak, peak and post-peak, which is marked by a black dash line and is also used to construct the *P-T* pseudosection diagram (Figure 6c,d).

The mineral assemblages identified in the petrographic observations include clinopyroxene, amphibole, plagioclase, epidote, quartz, ilmenite, and rutile. A *P-T* pseudosection for the sample MM-1 is constructed in the *P-T* range of 3-8 kbar and 400 ºC-800 ºC in the NCFMASHTO system (Figure 6c). Clinopyroxene in the pseudosection is pressure-dependent and continuously increases with pressure, and it becomes stable under higher temperature conditions. Amphibole is ubiquitous and stable in approximately all *P-T* fields. Plagioclase also mostly appears in the pseudosection. The significant occurrence of amphibole and plagioclase is supported by the presence of amphibole and plagioclase in petrographic thin sections. The epidote is present at higher pressures (4.5 kbar-8.0 kbar) and lower temperatures (400 ºC-600 ºC). To acquire the appropriate *P-T* conditions for metamorphism of the significant mineral assemblage, the isopleths of amphibole, clinopyroxene, and epidote are delineated on the pseudosection (Figure 6d). During pre-peak metamorphism, clinopyroxene grains contain epidote, amphibole, plagioclase, ilmenite, and rutile, as represented by the mineral assemblage Ep-Amp-Cpx-Pl-Ilm-Ru-Qz, which is stable at a *P-T* range of

5.5 kbar-8.0 kbar and 450 ºC-600 ºC. Amphibole, clinopyroxene, and epidote isopleths further narrow down the *P-T* conditions of the pre-peak metamorphic stage at 6.7 kbar and 510 ºC. The mineral assemblage of Amp-Cpx-Pl-Ilm-Ru-Qz characterizes the peak metamorphic stage. The epidote becomes unstable with increasing temperatures. This assemblage is stable in a *P-T* range of 7.2 kbar-8.0 kbar and 560 ºC-580 ºC. Isopleths of amphibole and clinopyroxene defined the *P-T* conditions for the peak metamorphic stage at P = 7.3 kbar and T = 578 ºC.

Later, the post-peak metamorphic stage is characterized by the mineral assemblage of Amp-Pl-Ilm-Ru-Qz, which acquires a Cpx free field. Due to a lowering in pressure, clinopyroxene is no longer stable at the post-peak metamorphic stage. This assemblage is stable under a *P-T* range of 3.0-5.0 kbar and 580 ºC-700 ºC. Isopleths of amphibole reveal the *P-T* conditions of the post-peak metamorphic stage at P = > 3.0 kbar and T = > 585 ºC.

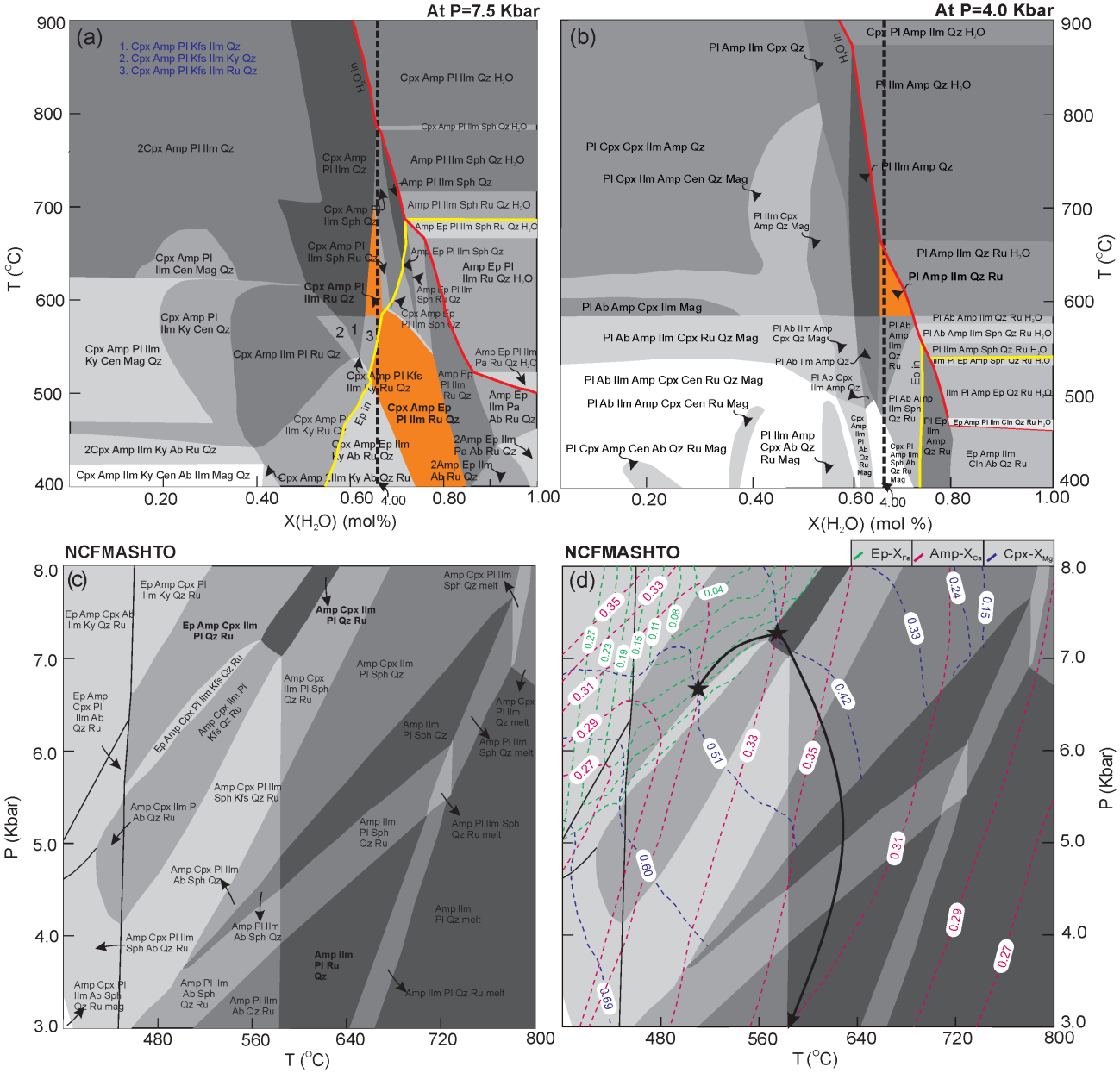

Figure 6. (a) T-X(H_2O) pseudosection at 7.5 Kbar, and (b) at 4.0 kbar, showing the effects of varying the molar proportions of bulk-rock H_2O (in MM-1). The black dashed line is the modelled composition of H_2O (4.00%). (c) *P-T* pseudosection showing pre-peak, peak and post-peak assemblages. (d) Isopleths X_{Ca} of Amp, X_{Mg} Cpx and X_{Fe} of Ep.

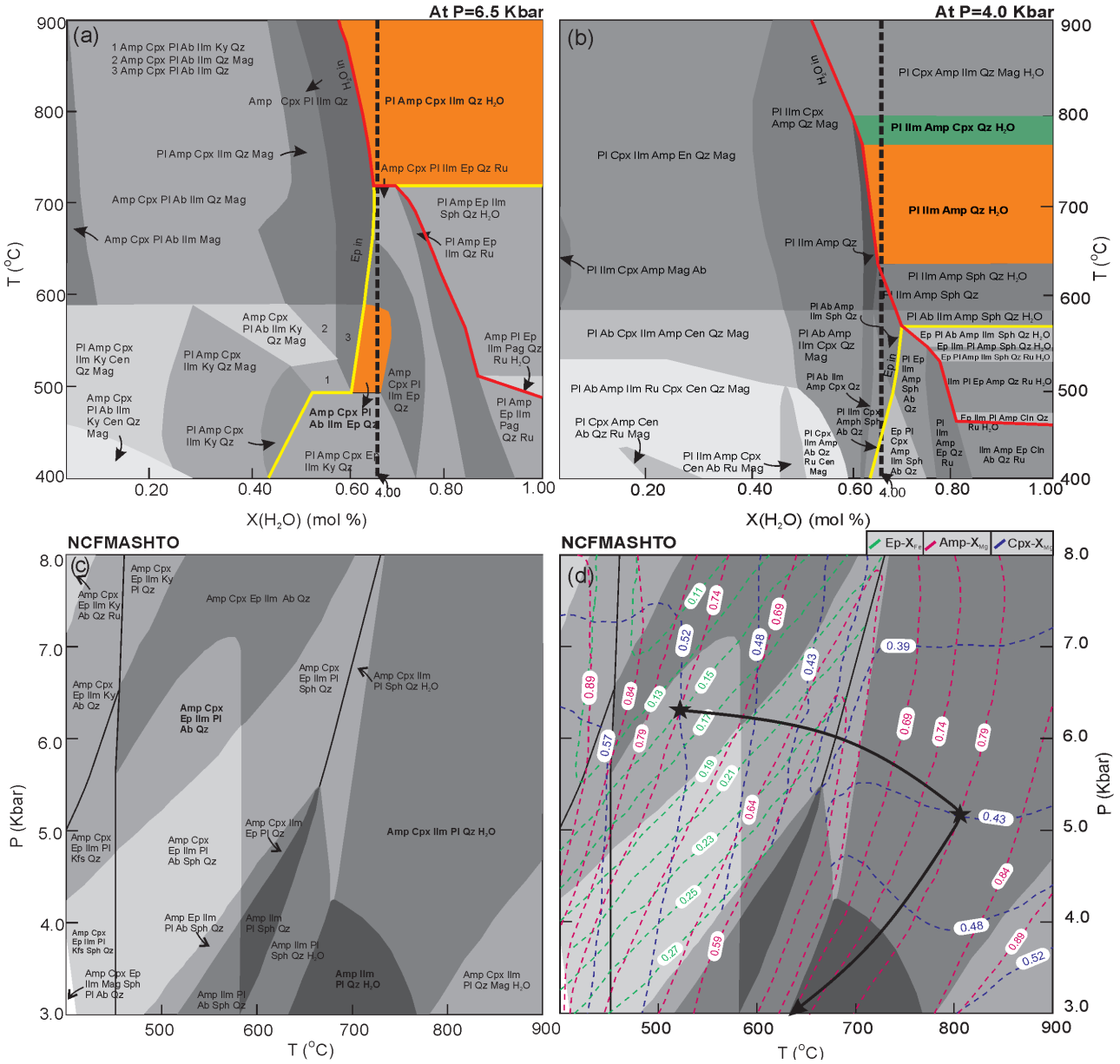

Figure 7. (a) T-X(H_2O) pseudosection at 6.6 Kbar and (b) at 4.0 Kbar, showing the effects of varying the molar proportions of bulk-rock H_2O in amphibolite (sample BB-1). The black dashed line is the modelled composition of H_2O (4.00%). (c) *P-T* pseudosection (sample BB-1) of amphibolites showing pre-peak, peak and post-peak metamorphic assemblages in the NCFMASTHO system. (d) Isopleths X_{Mg} of amphibole, X_{Mg} of clinopyroxene and X_{Fe} of epidote contouring *P-T* pseudosection.

6.4 Sample BB-1

The same process of computing H_2O values was repeated for sample BB-1. Table 8 shows how the necessary mole ratios of oxide are normalized to 100% in the NCFMASHTO system. At 6.5 and 4.0 kbar, a T-X(H_2O) pseudosection was also displayed (Figure 7a,b). The epidote is unstable at lower H_2O concentrations before breaching the Ep entry line, as seen in Figures 7a and 7b. As the temperature rises, the solid red line represents the emergence of H_2O. In X(H_2O) values of 0.60-0.65, the pre-peak mineral assemblage Ep-Amp-Cpx-Pl-Ab-Ilm-Qz remains stable (long dashed black line). While the mineral assemblage of the peak stage Amp-Cpx-Pl-Ilm-Qz-H_2O is stable for X(H_2O) values of 0.61-1.00, the mineral assemblage of the post-peak stage Amp-Pl-Ilm-Qz-H_2O does not appear in Figure 7a at a higher pressure of 6.5 kbar, and this is most likely owing to the pressure value chosen to be high. The post-peak and peak stage mineral assemblages became visible when the T-X(H_2O) diagram is calculated

at lower pressures of 4.0 kbar (Figure 7b). As a result, we chose an X(H_2O) value of 4.00, which was calculated using effective composition (Table 8) and then normalized to 100% in the NCFMASHTO system by considering stable fields of mineral assemblages for pre-peak, peak and post-peak, which is marked by a black dash line and is also used to construct the *P-T* pseudosection diagram (Figures 7c and 7d).

In the NCFMASHTO model system, a specific *P-T* pseudosection for the representative amphibolite sample (BB-1) has been generated in the *P-T* range of 3 kbar-8 kbar and 400 °C-900 °C (Figure 7c). In the pseudosection, clinopyroxene shows a pressure-dependent character and is stable at higher temperatures with other mineral phases such as amphibole, plagioclase, ilmenite, quartz, and H_2O. Amphibole is ubiquitous in all phases and is stable over a wide *P-T* range. Plagioclase is also found mostly in the pseudosection. Epidote can be found at high and low pressures (3.0 kbar-8.0 kbar), but only at much lower temperatures (> 680 °C). The most common Ti-bearing phases are ilmenite and magnetite. This rock is devoid of rutile. The *P-T* pseudosection of the BB-1 sample revealed three stages of metamorphism. The first is the pre-peak metamorphic stage, which is characterized by epidote, amphibole, plagioclase, and ilmenite inclusions inside clinopyroxene grains. This stage produces the mineral assemblage Ep-Amp-Cpx-Pl-Ab-Ilm-Qz, stable in the pseudosection at *P-T* ranges of 4.8 kbar-7.0 kbar and 450 °C-580 °C. *P-T* conditions of the pre-peak metamorphic stage at P = 6.27 kbar and T = 520 °C are further constrained by isopleths of amphibole, clinopyroxene, and epidote (Figure 7d). The peak metamorphic stage is defined by the mineral assemblage Amp-Cpx-Pl-Ilm-Qz-H_2O. With the rising temperature, the epidote becomes unstable, and H_2O forms at a higher temperature. This assemblage obtains a field with a *P-T* of 3.0 kbar-8.0 kbar and a temperature of 680-900 °C. The *P-T* conditions of the peak metamorphic stage at P = 5.2 kbar and T = 805 °C are further narrowed by isopleths of amphibole and clinopyroxene. Finally, the mineral assemblage Amp-Pl-Ilm-Qz-H_2O denotes the post-peak metamorphic stage. At the post-peak metamorphic stage, clinopyroxene is no longer stable. This assemblage acquires a field with a *P-T* of 3.0 kbar-4.2 kbar and a temperature of 620 °C-780 °C and is further defined as > 3.0 kbar and > 640 °C by the isopleths of amphibole.

7. Discussion

The Mauranipur and Babina amphibolites were chosen for this investigation because they demonstrate medium to high-grade metamorphism in the BuC. The BuC amphibolites are primarily found in the Mauranipur-Babina region as enclaves within the TTGs. The mineralogical assemblage of amphibolites is Hbl + Cpx + Pl ± Qz ± Ep [46]. The geochemistry of amphibolites from the CBGT was also previously studied. According to their findings, tholeiitic magma is the primary source of amphibolites [34]. The Nd isotopic values of amphibolites provide two model ages: one for the protolith of amphibolites, 4.9-4.2 Ga, and the other for amphibolites metamorphism, 3.4-3.3 Ga [31]. Based on the Nd levels, the amphibolites were generated in a subduction-related environment. Many researchers have postulated a subduction zone context for the evolution of the BuC based on the analysis of TTGs, granitoids, amphibolites, basaltic, and komatiitic rocks [34]. A geodynamic model for the evolution of the CBGT based on observations of exposed mafic-ultramafic rocks in the Babina and Mauranipur regions was also explained earlier [31]. The presence of mafic-ultramafic rocks, metabasic rocks, amphibolites, BIFs, and meta-sediments in CBGT shows that they are remains of earlier oceanic crust. At 2.7 Ga, the oceanic plate subducted, causing the melting of mafic rocks containing garnet and water, which reacted with the mantle, forming the TTGs [47].

Three metamorphic stages have been identified based on mineral assemblages, textural correlations, and *P-T* pseudosections. The creation of isopleths on the *P-T* pseudosection defines the *P-T* conditions of these three metamorphic stages. For amphibolites from the Mauranipur and Babina regions, they have set up a clockwise *P-T* path. Figures 6d and 7d demonstrate the *P-T* pathways of Mauranipur and Babina amphibolites, respectively. The *P-T* routes of both amphibolites follow a similar pattern, although the *P-T* conditions of the different metamorphic stages differ significantly. Mauranipur amphibolites reach a pre-peak metamorphic stage at a lower pressure and temperature (6.7 kbar, 510 °C) than Babina amphibolites (6.27 kbar, 520 °C). Peak metamorphism occurs in Babina amphibolites at 5.2 kbar/805 °C, substantially higher in temperature and pressure than the peak metamorphic *P-T* conditions in Mauranipur amphibolites (7.3 kbar/578 °C). Due to the availability of rutile, these differences may be conceivable. Similarly, Mauranipur amphibolites' post-peak metamorphic stage is defined by a *P-T* condition of > 3.0 kbar/ > 585 °C, which is similar in pressure but lower in temperature than Babina amphibolites (> 3.0 kbar/ > 640 °C). Ep-Amp-Cpx-Pl-Ilm-Ru-Qz and Ep-Amp-Cpx-Pl-Ilm-Ab-Qz mineral assemblages characterize the pre-peak stage of Mauranipur and Babina amphibolites, respectively. In the Mauranipur region, rutile is found in both a pre-peak and a peak metamorphic state, but it is rare in amphibolites from the Babina region. Rutile is a stable mineral in medium- to high-grade metamorphic belts and serves as a clue material for subduction tectonic environments [48].

Following that, both locations were further buried, resulting in a constant rise in pressure and temperature, and amphibolites underwent peak metamorphism, generating mineral assemblages of Amp-Cpx-Pl-Ilm-Ru-Qz and Amp-Cpx-Pl-Ilm-Qz-H_2O in the Mauranipur and Babina regions, respectively. Under a decompression procedure, a post-peak stage followed this peak stage, with a reduction in pressure conditions. The presence of the mineral assemblages Amp-Pl-Ilm-Ru-Qz (MM-1) and Amp-Pl-Ilm-Qz-H_2O (BB-1) in the post-peak stage indicates that it was formed by the decompression and subsequent exhumation of amphibolites on the surface.

8. Conclusions

1) *P-T* pseudosections for amphibolites from both regions are plotted in the NCFMASHTO system and characterized by three metamorphic stages.
2) The pre-peak, peak, and post-peak stages of amphibolites of the Mauranipur are designated by the presence of mineral assemblages Ep-Amp-Cpx-Pl-Ilm-Ru-Qz, Amp-Cpx-Pl-Ilm-Ru-Qz, and Amp-Pl-Ilm-Ru-Qz, respectively. However, the pre-peak, peak, and post-peak stages of amphibolites of the Babina are demarcated by the mineral assemblage Ep-Amp-Cpx-Pl-Ab-Ilm-Qz, Amp-Cpx-Pl-Ilm-Qz-H_2O, and Amp-Pl-Ilm-Qz-H_2O, respectively.
3) The *P-T* condition of the pre-peak stage is 6.7 kbar/510 ºC, the peak stage is 7.3 kbar/578 ºC, and the post-peak stage is > 3.0 kbar/> 585 ºC in the Mauranipur amphibolites. Similarly, the *P-T* condition of the pre-peak stage is 6.27 kbar/520 ºC, the peak stage is 5.2 kbar/805 ºC, and the post-peak stage is > 3.0 kbar/> 640 ºC in the Babina amphibolites.
4) Amphibolites of both regions show a clockwise *P-T* path, suggesting burial followed by exhumation.

Authors' Contributions

Pratigya Pathak: Field sampling, Conceptualization, Analysis, Investigation, Writing-original draft. **Shyam Bihari Dwivedi:** Supervision, Reviewing and Editing. **Ravi Ranjan Kumar:** Conceptualization, Writing-original draft.

Conflicts of Interest

On behalf of all authors, the corresponding author would like to declare that this manuscript does not have any conflict of interest whatsoever following the Policy of the Journal of Environment and Earth Sciences.

Acknowledgements

The authors thank the Director, Indian Institute of Technology (BHU), for providing the infrastructure to carry out our work. We are grateful to the Ministry of Human Resource Development (MHRD) Fellowship Scheme for providing financial support. The author expresses her gratitude to Prof. R.K. Srivastava and Dr. G.C. Gautam from the Department of Geology, Banaras Hindu University (India), for facilitating the Microscopy Laboratory.

References

[1] Iizuka, T., Horie, K., Komiya, T., et al., 2006. 4.2 Ga zircon xenocryst in an Acasta gneiss from northwestern Canada: Evidence for early continental crust. Geology. 34, 245-248.
[2] Wilde, S.A., Valley, J.W., Peck, W.H., et al., 2001. Evidence from detrital zircons for the existence of continental crust and oceans on the Earth 4.4 Gyrago. Nature. 409, 175-178.
[3] Zeh, A., Stern, R., Gerdes, A., 2014. The oldest zircons of Africa—their U-Pb-Hf-O isotope and trace element systematics, and implications for Hadean to Archaean crust-mantle evolution. Precambrian Research. 241, 203-230.
[4] Armstrong, R.L., 1981. Radiogenic isotopes: The case for crustal recycling on a near steady-state-no-continental growth Earth. Philosophical Transactions Royal Society London. 301, 443-472.
[5] Dhuime, B., Hawkesworth, C.J., Cawood, P., 2011. When continents formed. Science. 331, 154-155.
[6] Guitreau, M., Blichert-Toft, J., Mojzsis, S.J., et al., 2014. Lu-Hf isotope systematics of the hadean–Eoarchean Acasta gneiss complex (northwest territories, Canada). Geochimica et Cosmochimica Acta. 135, 251-269.
[7] Pearce, J.A., 2014. Geochemical fingerprinting of the Earth's oldest rocks. Geology. 42, 175-176.
[8] Pearce, J.A., Peate, D.W., 1995. Tectonic implications of the composition of volcanic arc magmas. Annual Review on Earth Planet Sciences. 23, 251-285.
[9] Naqvi, S.M., 2005. Geology and evolution of the Indian plate (from Hadean to Holocene—4 Ga to 4 Ka). Capital Publishing Company: New Delhi. pp. 450.
[10] Condie, K.C., Davaille, A., Aster, R.C., et al., 2015. Upstairs-downstairs: Supercontinents and large igneous provinces, are they related? International Geology Review. 57, 1341-1348.
[11] Saha. L., Pant, N.C., Pati, J.K., et al., 2011. Neo-

archean high-pressure margarite-phengitic muscovite-chlorite corona mantled corundum in quartz-free high-Mg, Al phlogopite-chlorite schists from the BundelkhandCraton, north-central India. Contribution to Mineralogy and Petrology. 161, 511-530.

[12] Kumar, S., Raju, S., Pathak, M., et al., 2010. Magnetic susceptibility mapping of felsic magmatic litho units in the central part of Bundelkhand massif, central India. Journal of Geological Society of India. 75, 539-548.

[13] Joshi, K.B., Bhattacharjee, J., Rai, G., et al., 2017. The diversification of granitoids and plate tectonic implications at the Archaean-Proterozoic boundary in the Bundelkhand Craton, central India. Geological Society Special Publication. 449, 123-157.

[14] Singh, S.P., Dwivedi, S.B., 2009. Garnet-sillimanite-cordierite-quartz-bearing assemblages from early Archean supracrustal rocks of Bundelkhand massif, Central India. Current Science. 97, 103-107.

[15] Singh, S.P., 2012. Archean geology of Bundelkhand craton, Central India: An overview. Gondwana Geological Magzine. 13, 125-140.

[16] Nasipuri, P., Saha, L., Hangqiang, X., et al., 2019. Paleoarchean crustal evolution of the Bundelkhand Craton, north Central India. Earth's Oldest Rocks. 31, 793-817.

[17] Raza, M.B., Nasipuri, P., Saha, L., et al., 2021. Phase relations and in-situ U-Th-Pb total monazite geochronology of Banded Iron Formation, Bundelkhand Craton, North-Central India, and their geodynamic implications. International Journal of Earth Sciences. 1-29.

[18] Pathak, P., Dwivedi, S.B., Kumar, R.R., 2022. Geochemistry and Phase equilibrium modelling of garnet-biotite gneiss from Mauranipur, Bundelkhand Craton, Northern India; implication for tectonic setting and metamorphism. Journal of Geosciences Research. Under Review.

[19] Singh, S.P., Dwivedi, S.B., 2015. High-grade metamorphism of the Bundelkhand massif and its implications for crustal evolution of the middle archean crust of central India. Journal of Earth System Science. 124, 197-211.

[20] Slabunov, A., Singh, V., 2019. Meso-Neoarchean crustal evolution of the BundelkhandCraton, Indian Shield: New data from greenstone belts. International Geology Review. 61, 1409-1428.

[21] Bhowmik, S.K., Ao, A., 2016. Subduction initiation in the Neo-Tethys: Constraints from counterclockwise P-T paths in amphibolite rocks of the Nagaland Ophiolite Complex, India. Journal of Metamorphic Geology. 34(1), 17-44.

[22] Somesha, G.S., Govindaraju, M.V., Govindaiah, S., 2019. Petrochemistry and pt condition of amphibolites associated with pegmatites of holenarasipura and karighatta schist belts of Western Dharwar Craton, Karnataka, India. International Journal of Science Technology and Research. 8, 570-580.

[23] Meshram, T., Shukla, D., Behera, K., et al., 2017. Petrography and geochemistry of the Amphibolites from the southeastern part of Yerapalli schist belt, Eastern Dharwar Craton, India. Journal of Indian Geophysical Union. 21, 391-400.

[24] Rajendran, S., Thirunavukkarasu, A., Poovalinga, B., et al., 2007. Petrological and geochemical studies of amphibolites in parts of Salem District, Tamil Nadu, India. Indian Mineralogist. 41, 169-175.

[25] Fanka, A., Sutthirat, C., 2018. Petrochemistry, mineral chemistry, and pressure-temperature model of corundum-bearing amphibolite from Montepuez, Mozambique. Arabian Journal for Science and Engineering. 43, 3751-3767.

[26] Kumar, R.R., Kawaguchi, K., Dwivedi, S.B., et al., 2022. Metamorphic evolution of the pelitic and mafic granulites from Daltonganj, Chhotanagpur Granite Gneiss Complex, India: Constraints from zircon U–Pb age and phase equilibria modelling. Geological Journal. 57(3), 1284-1310.
DOI: https://doi.org/10.1002/gj.4340

[27] Basu, A.K., 1986. Geology of parts of the Bundelkhand Granite massif Central India. Record of Geological Survey of India. 117, 61-124.

[28] Bhattacharya, A.R., Singh, S.P., 2013. Proterozoic crustal scale shearing in the Bundelkhand massif with special reference to quartz reefs. Journal of the Geological Society of India. 82, 474-484.

[29] Absar, N., Raza, M., Roy, M., et al., 2009. Composition and weathering conditions of the Paleoproterozoic upper crust of Bundelkhand craton, Central India: records from the geochemistry of clastic sediments of 1.9 Ga Gwalior Group. Precambrian Research. 168, 313-329.

[30] Singh, P.K., Verma, S.K., Singh, V.K., et al., 2021. Geochronology and petrogenesis of the TTG gneisses and granitoids from the Central Bundelkhand granite-greenstone terrane, BundelkhandCraton, India: Implications for Archean crustal evolution and cratonization. Precambrian Research. 359, 106-210.

[31] Singh, P.K., Verma, S.K., Moreno, J.A., et al., 2019. Geochemistry and SmNd isotope systematics of mafic-ultramafic rocks from the Babina and Mauranipur greenstone belts, Bundelkhand Craton, India: Impli-

cations for tectonic setting and Paleoarchean mantle evolution. Lithos. 330, 90-107.

[32] Singh, V., Slabunov, A., Svetov, S., et al., 2018. Occurrence of archean iron bearing rocks from Babina, Mauranipur and Girar Area of the Bundelkhand Region: As potential reserves. Archaeology Anthropology Open Access. 3, 108-113.

[33] Pandey, U.K., Bhattacharya, D., Shastry, D.V.L.N., et al., 2011, Geochronology Rb-Sr, Sm-Nd and Pb-Pb, isotope geochemistry and evolution of the granites and andesites hosting Mohar Cauldron, Bundelkhand Granite Complex, Shivpuri district, Central India. Exploration Research on Atomic Minerals. 21, 103-116.

[34] Singh, V.K., Slabunov, A., 2015. The Central Bundelkhand Archaean greenstone complex, Bundelkhand craton, central India: Geology, composition, and geochronology of supracrustal rocks. International Geology Review. 57(11-12), 1349-1364.

[35] Leake, B.E., Woolley, A.R., Arps, C.E.S., et al., 1997. Nomenclature of amphiboles: Report of the subcommittee on amphiboles of the international mineralogical association, commission on new minerals and mineral names. Canadian Mineral. 35, 219-246.

[36] Morimoto, N., 1988. The nomenclature of pyroxenes. Mineral Magzine. 52, 425-433.

[37] Tarantola, A., Voudouris, P., Eglinger, A., et al., 2019. Metamorphic and metasomatic kyanite-bearing mineral assemblages of Thassos Island (Rhodope, Greece). Minerals. 9(4), 252.

[38] Connolly, J.A.D., 2005. Computation of phase equilibria by linear programming: A tool for geodynamic modelling and its application to subduction zone decarbonization. Earth Planet Science Letters. 236, 524-541.

[39] Connolly, J.A.D., 2009. The geodynamic equation of state: What and how. Geochemical Geophysical Geosystems. 10(10), 1-19.

[40] Holland, T.J.B., Powell, R.T.J.B., 1998. An internally consistent thermodynamic data set phases of petrological interest. Journal of Metamorphic Geology. 16(3), 309-343.

[41] Holland, T.J.B., Powell, R., 2011. An improved and extended internally consistent thermodynamic dataset for phases of petrological interest, involving a new equation of state for solids. Journal of Metamorphic Geology. 29, 333-383.

[42] Green, E.C.R., White, R.W., Diener, J.F.A., et al., 2016. Activity-composition relations for the calculation of partial melting equilibria in metabasic rocks. Journal of Metamorphic Geology. 34(9), 845-869.

[43] Diener, J.F.A., Powell, R., White, R.W., et al., 2007. A new thermodynamic model for clino- and orthoamphiboles in the system Na_2O-CaO-FeOMgO-Al_2O_3-SiO_2-H_2O-O. Journal of Metamorphic Geology. 25(6), 631-656.

[44] Holland, T.J.B., Powell, R., 2003. Activity-composition relations for phases in petrological calculations: an asymmetric multi-component formulation. Contribution to Mineralogy and Petrology. 145, 492-501.

[45] White, R.W., Powell, R., Holland, T.J.B., et al., 2000. The effect of TiO_2 and Fe_2O_3 on metapelitic assemblages at greenschist and amphibolite facies conditions: Mineral equilibria calculations in the system K_2O-FeO-MgO-Al_2O_3-SiO_2-H_2O-TiO_2-Fe_2O_3. Journal of Metamorphic Geology. 18, 497-511.

[46] Pati, J.K., 2020. Evolution of Bundelkhand craton. Episodes. 43(1), 69-87.

[47] Verma, S.K., Verma, S.P., Oliveira, E.P., et al., 2016. LA-SF-ICP-MS zircon U-Pb geochronology of granitic rocks from the central Bundelkhand greenstone complex, Bundelkhand craton, India. Journal of Asian Earth Science. 118, 125-137.

[48] Meinhold, G., 2010. Rutile and its applications in earth sciences. Earth-Science Reviews. 102, 1-28. DOI: https://doi.org/10.1016/j.earscirev.2010.06.001

[49] Whitney, D.L., Evans, B.W., 2010. Abbreviations for names of rock-forming minerals. American Mineralogist. 95, 185-187.